Significant local sea level variations caused by continental hydrology signals

Rebecca McGirr[1,2], Paul Tregoning[1,2], Anthony Purcell[1], Herb McQueen[1]

[1]Research School of Earth Sciences, Australian National University, Canberra, ACT, 0200, Australia
[2]The Australian Centre for Excellence in Antarctic Science, University of Tasmania, Hobart, Tasmania 7001, Australia

Key Points:

- Exchange of water between continents and oceans causes global sea level change at rates comparable to the contributions of ice sheets
- The direct gravitational attraction effect on local sea level is of a larger magnitude than the far-field sea level changes
- Inter-annual continental hydrology signal impacts on local sea level have negated the impacts of melting polar ice sheets in some locations

Corresponding author: Rebecca McGirr, `rebecca.mcgirr@anu.edu.au`

Abstract

Space gravity missions have enabled the quantification of the mass component of sea-level rise over the past two decades. Barystatic sea-level rise is predominantly driven by melting polar ice sheets and mountain glaciers. However, continental hydrological processes also contribute to global sea level change at significant magnitudes. We show that for most coastal areas in low-to-mid latitudes, up to half of manometric sea-level rise is due to changes in water storage in ice-free continental regions. At other locations the direct attraction effect of anthropogenic pumping of groundwater over the duration of the GRACE and GRACE-FO mission offsets sea-level rise from ice sheet and glacier melt. If these trends in continental hydrological storage were to slow or stop, these regions would experience greatly accelerated sea-level rise, posing a risk to coastal settlements and infrastructure, however, for most coastal communities current rates of sea-level rise would be significantly reduced.

Plain Language Summary

It is well understood that melting of polar ice sheets and mountain glaciers cause increases in ocean mass, leading to a corresponding rise in global sea level. What is not as obvious is that multi-year changes in the storage of water on continents not covered by ice also contribute significantly to changes in global sea level. Over recent years and in some locations, the magnitude of these 'continental hydrology' contributions to sea level changes have been comparable to the contributions of the ice-covered regions. In some cases, the former have offset the ice sheet contributions, thus reducing regional sea-level rise to substantially smaller magnitudes. Through an analysis of space gravity data, we have quantified the effects of continental hydrology on regional sea level and show that changes caused both naturally (e.g. through La Niña events) and through anthropogenic activities (e.g. extraction of groundwater) can increase or decrease regional sea level by significant amounts.

1 Introduction

Increases in ocean mass have resulted in global mean sea level (GMSL) rising at ∼2.5 mm/yr from 2005 to 2017 (Tapley et al., 2019); however, the most important impact of sea-level variations on society lies in the regional sea-level changes rather than global averages. The mass component of GMSL rise, referred to as barystatic sea-level rise (Gregory et al., 2019), is predominantly caused by continental freshwater fluxes, including mass balance change of ice sheets (Velicogna & Wahr, 2013; Tapley et al., 2019) (Greenland and Antarctica) and mountain glaciers (Wouters et al., 2019; Ciracì et al., 2020) (e.g. Alaska, Patagonia, Svalbard), and changes in terrestrial water storage (TWS), which includes groundwater storage, soil moisture, and natural and artificial surface water storage (Leblanc et al., 2009; Rodell et al., 2018; Frappart et al., 2019). Closure of the ocean mass budget has been the focus of many studies (e.g., Barnoud et al., 2023) and involves the apportioning of contributions from polar ice sheets, mountain glaciers, and the components of TWS. Rather than considering regional ocean mass changes (referred to as manometric sea level) (Gregory et al., 2019), studies of this process tend to take a global approach. This is achieved using a combination of ocean height changes measured by satellite altimetry corrected for steric sea-level changes derived from ocean temperature and salinity observations, and ocean mass change from space gravity missions.

Exchanges of water between continents and oceans includes three additional components that directly affect relative sea-level changes beyond the simple volumetric effect. First, variations in the water mass on the continent change the direct gravitational attraction between the oceans and continents (Mitrovica et al., 2001; Lambeck et al., 2017). This process can have a significant effect on local sea level near the location of change of continental water source (J. Sun et al., 2022). Second, water added or taken from the oceans moves the centre of mass of the Earth and is redistributed on a rotating Earth according to particular spatial patterns (Mitrovica et al., 2001; Tamisiea et al., 2010) and affects sea level in the far-field. Third, elastic deformation of the ocean floor occurs due to changing ocean mass loads (Mitrovica et al., 2001, 2011), affecting both near-field and far-field ocean heights. Sea level gravitational, rotational and deformational (GRD) fingerprints (Tamisiea et al., 2010; Kim et al., 2019; J. Sun et al., 2022) can be used to calculate the spatial pattern of ocean height changes related to mass changes on land.

The Gravity Recovery and Climate Experiment (GRACE) and GRACE Follow-On (GRACE-FO) space gravity missions provide near-continuous data from 2002 to present from which estimates of change in mass distribution on Earth can be made (Tapley et al., 2004, 2019). The leakage of signals between continents and oceans has been problematic in the analysis of space gravity data when estimating changes in mass distribution (Velicogna & Wahr, 2006; Chen et al., 2009). Various re-scaling strategies have been invoked (Watkins et al., 2015; Wiese et al., 2016), as well as novel forward modelling approaches to re-instate leaked signal back to the likely correct location on the continents (Chen et al., 2009; Jeon et al., 2021). Recently, Goux et al. (2023) developed a diffusion filter which mitigates signal leakage by conserving mass within defined boundaries. The use of mass concentration elements (mascons) (Muller & Sjogren, 1968), rather than spherical harmonics, helps to reduce the leakage of signal by permitting more direct spatial constraints on parameters to be applied (Rowlands et al., 2005; Watkins et al., 2015; Tregoning et al., 2022). Irregular-shaped mascons, that follow coastlines with an accuracy of <9 km, further reduce the leakage of signal between continents and oceans (Tregoning et al., 2022).

During the GRACE mission (2002-2016) the Greenland (0.77 mm/yr) and Antarctic (0.33 mm/yr) ice sheets were the largest contributors to barystatic sea-level rise (Rodell et al., 2018). Using a forward modelling approach, Kim et al. (2019) estimated that TWS changes contributed 0.32 mm/yr to GMSL between 2005 and 2016, leading to tighter closure of the ocean mass budget. Through the use of forward modelling of GRACE estimates of TWS change and sea-level fingerprints, agreement was found between regional ocean height changes and those observed by satellite altimetry (Jeon et al., 2021). Satellite gravity data has enabled identifying the source of inter-annual variations in GMSL. For example, a drop in GMSL of several millimetres from mid-2010 to early 2011 is visible in the GRACE record and steric-corrected altimetry measurements (Boening et al., 2012). This fall in sea level coincided with a strong negative phase of the El Niño Southern Oscillation (ENSO) index, which resulted in significant rainfall over large portions of northern South America and the Australian landmass (Boening et al., 2012).

By separating the contributions from ice-covered regions and other continental areas, we can conduct a more detailed assessment of how continental hydrological processes influence the spatial pattern of sea-level change. The latter includes groundwater variations, changes in soil moisture volumes, and changing volumes in natural (lakes, rivers) and artificial (reservoirs) surface water storage. To quantify these effects, we analyse GRACE and GRACE-FO measurements to assess the integrated change of TWS components and the mass balance of ice sheets and glaciers. These continental mass changes are then convolved with sea-level GRD fingerprints to construct time series of ocean mass changes. These computed GRD values serve as a basis for identifying the relative contributions of continental hydrology sources and mass balance changes to both local sea level at specific locations and the global pattern of manometric sea-level change.

2 Space gravity data analysis

We estimate changes in mass on Earth as a change in height of a water column on 12,755 irregularly shaped mascons using the range acceleration as the key inter-satellite observation of the GRACE and GRACE Follow-On space gravity missions (Allgeyer et al., 2022). Data from August 2002 to September 2023 were processed, using the hybrid ACH1B data to model the non-gravitational accelerations on the GRACE-D satellite (Harvey et al., 2022). Non-linear effects in accelerometer measurements, caused by thermal variations within the satellites, were mitigated using a high-pass filtering approach (McGirr et al., 2022). This enables the number of accelerometer calibration parameters to be limited to one bias and one scale per day per orthogonal axis for the GRACE and GRACE-FO data. We computed degree-1 contributions using a combination of GRACE and ocean model data (Y. Sun et al., 2016), replacing $C_{2,0}$ estimates with values derived from satellite ranging data, and updating $C_{3,0}$ values for GRACE-FO data (Loomis et al., 2020). Our solutions have also been corrected for glacial isostatic adjustment using the ICE6G_D model (Peltier et al., 2018) and the AOD1B-GAD product (Dobslaw et al., 2017). We formed normal equations for 24-hour orbital arcs, then stacked these daily normal equations to form monthly solutions, defined using calendar months.

To mitigate inherent noise in space gravity data inversions, we regularise solutions using consistent values across mascons within broad spatial regions. The off-diagonal elements of our regularisation matrix are zero and the diagonal elements are $1/\sigma^2$ as shown in Figure S1. The regularisation matrix is applied for each day included in the monthly solution and we use the same regularisation for each monthly solution to keep the analysis process as generic as possible. The mascon parameter uncertainties are defined as the standard deviations obtained from the variance-covariance matrix of the regularised least squares inversion.

3 Calculation of GRD ocean mass change

For a meter change in water storage on each land mascon, we calculated the corresponding change in water height of each ocean mascon. We employed the algorithm described by Lambeck et al. (2017), which calculates the solid Earth's response to load changes and solves the sea-level equation for an elastic Earth (Farrell & Clark, 1976). We included the gravitational, rotational and elastic deformation signals caused by the mass exchange between land and oceans to calculate the sea-level GRD fingerprints. The computations were done on a radially symmetric, spheroidal elastic Earth using the elastic structure of the Preliminary Reference Earth Model (Dziewonski & Anderson, 1981). Visco-elastic effects were not included because the magnitudes of load variations are small (<15 m) and the time scale of the variations is short (<1 month).

The GRACE and GRACE-FO mascon solutions of monthly mass changes on land were multiplied by the computed sea-level GRD fingerprints to apportion the signals over the oceans, thus deriving corresponding monthly ocean signals (which we refer to as computed GRD values). The uncertainties of the computed GRD values for each ocean mascon for each month were calculated by propagating the monthly formal uncertainties of the continental mascons using the GRD fingerprints. Subsequently, we determined the computed GRD contribution to manometric sea-level trends from August 2002 to September 2023 for each ocean mascon using a least squares regression of the computed GRD values weighted by the propagated uncertainties. To increase the accuracy of trend estimation, we included modelling of annual and semi-annual signals in our regression analysis and chose not to fill the GRACE to GRACE-FO mission gap with modelled data to avoid introducing artificial trends.

We computed GRD values separately for ocean mass changes caused by ice-covered and ice-free regions. To isolate continental hydrology signals from ice-related signals over continents, we excluded mass changes over Greenland, Antarctica, the Alaskan and Patagonian glaciers as well as the ice-covered regions of Northeast Canada (Baffin Island, Ellesmere Island), Svalbard and Russian Arctic islands (Severnaya Zemlya and Novaya Zemlya).

We also computed the GRD values of six ice-free regions to understand separately each continents contributions to ocean mass change (Figure S2).

4 Ocean mass from satellite altimetry

The spatial variability of the contributions of both ice-based and continental hydrology to ocean mass change creates a complex pattern from which to extract a comprehensive synthesis of local information. Ocean dynamic sea level further complicates this pattern, redistributing ocean mass according to atmosphere-ocean circulation variations. While the computed GRD changes in sea level do not include the impacts of atmosphere-ocean circulation, these variations are captured in GRACE/GRACE-FO ocean mascon estimates and altimetry ocean height anomalies. To understand the impact of both ocean dynamic sea level and computed GRD values, we analysed ocean mass change from our estimated ocean mascons and steric-corrected altimetry. We utilised altimetry-based datasets of barystatic and gridded 0.5° manometric sea level with monthly temporal resolution (Barnoud et al., 2023). These datasets include satellite altimetry sea-level anomalies (Legeais et al., 2021) corrected for a drift in the Jason-3 microwave radiometer wet troposphere correction (Barnoud et al., 2023) and thermosteric sea level computed from various in-situ temperature and salinity datasets (e.g., Good et al., 2013; Cheng et al., 2017).

We analysed the difference between barystatic and manometric sea level from the computed GRD values, estimated ocean mascons and steric-corrected altimetry during the common data period (August 2002 to December 2020). We computed barystatic sea level using satellite gravity data by integrating our estimated ocean mascons and computed GRD values for all landmasses over the global ocean, excluding areas not well sampled by Argo data (i.e. polar oceans and marginal seas) and coastal areas poorly resolved by satellite altimetry (Legeais et al., 2021; Barnoud et al., 2023). We compared ice-free manometric sea-level changes of the computed GRD values with our ocean mascon estimates and steric-corrected altimetry at particular locations where the rates of continental hydrology contributions were high. Annual and semi-annual signals were removed using a weighted least squares regression to analyse the ocean mass trends and inter-annual variations.

5 Results

5.1 Contributions to ocean mass change

Continental hydrology signals in ice-free regions (Figure 1a,c) contributed 25% (0.5 ± 0.04 mm/yr) to barystatic sea level (2002-2023), with the remaining portion (75%; 1.5 ± 0.01 mm/yr) accounted for by melting mountain glaciers and ice-sheets which are predominantly found at high latitudes (Figure 1b,c). Although the contribution of ice-covered regions to GMSL is $\sim$3-times greater than ice-free regions, these continental hydrology signals contributed significantly to rates of manometric sea level in some locations by mitigating or amplifying ocean mass increase due to ice melt. The rate of manometric sea-level change from continental hydrology over the GRACE and GRACE-FO era has a distinct spatial pattern driven predominantly by total TWS trends in Asia (Figure 1a). Meanwhile, the spatial pattern due to ice-melt caused near-uniform sea-level rise in mid-to-low latitude areas (Figure 1b).

Declining TWS in Asia over the GRACE/GRACE-FO era led to an increase of $\sim$0.9 mm/yr across the central Atlantic Ocean, the North Pacific Ocean, around Africa, Australia and surrounding Pacific Island nations (Figure 1a0). The significant reductions in continental hydrology contributions to ocean mass in the Black Sea, eastern Mediterranean Sea and the Persian Gulf were caused by decreased strength in the direct gravitational attraction due to declining TWS in Asia since 2002, including around -0.1 mm/yr due to decreased water storage in the Caspian Sea. Although typically less than 1 mm/yr,

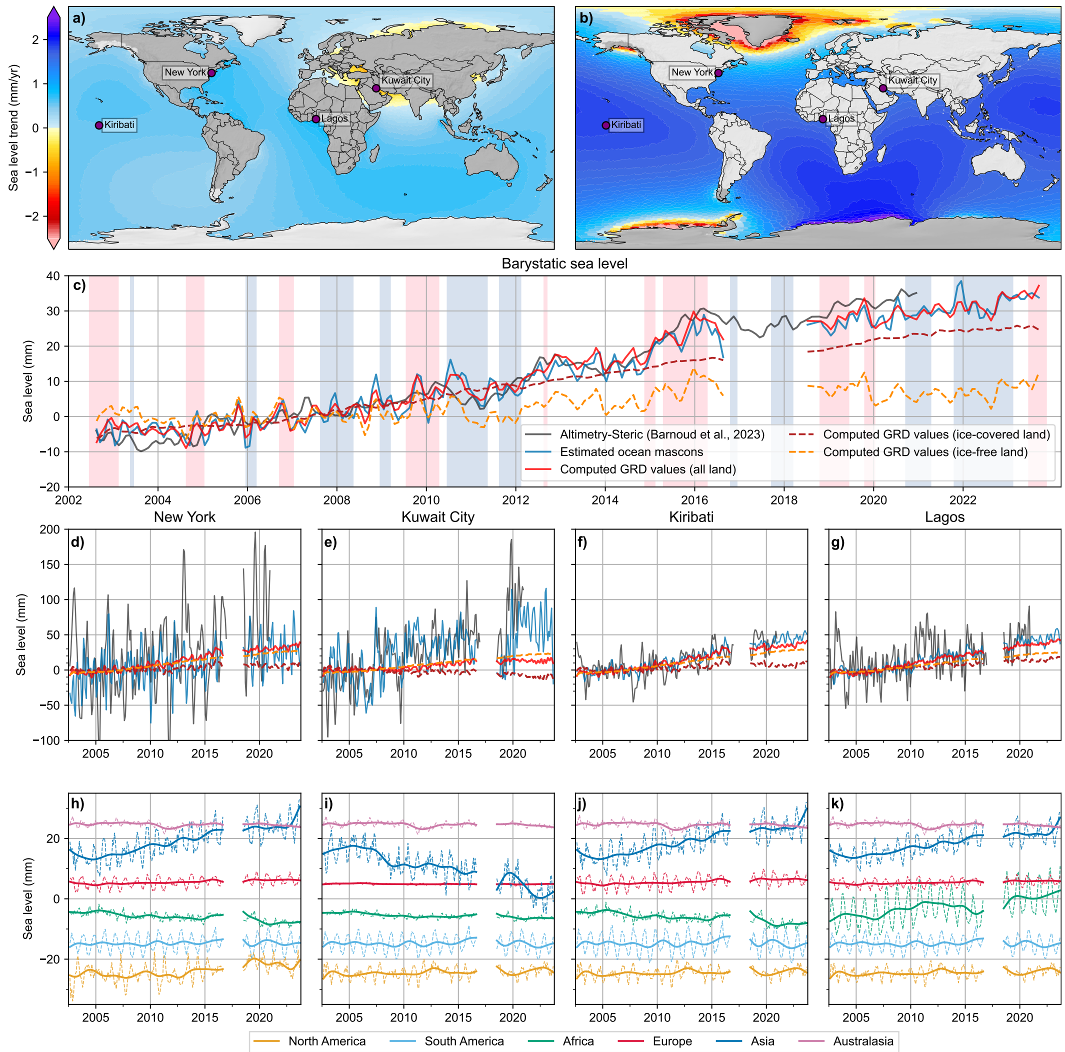

Figure 1. Trends in computed GRD values of ocean mass change (August 2002 to September 2023) in mm/yr of sea level due to (a) ice-free land and (b) ice-covered land (dark grey regions). Trend uncertainties are provided in Figure S3. (c) Barystatic sea level with annual and semiannual signals removed from steric-corrected altimetry (Barnoud et al., 2023) (black), our estimated ocean mascons (blue) and computed GRD values for all land masses (red), ice-covered land (orange), ice-free land (purple). Red and blue vertical bars indicate El Niño and La Niña events, respectively (Rayner et al., 2003). (d-g) Manometric sea level at four locations, legend as per (b). (h-k) Contributions of six ice-free continental regions to changes in manometric sea level at each location (dashed line) and 24-month low-pass filtered values (solid line) (offset by 10 mm).

local ocean mass changes driven by continental hydrology were comparable to or greater than individual contributions of the Greenland (-0.66±0.01 mm/yr) and Antarctic (-0.39±0.01 mm/yr) ice sheets to GMSL over the study period.

Our satellite gravity-based estimates of barystatic sea level contain more high-frequency variations compared to steric-corrected altimetry (Barnoud et al., 2023). However, interannual variations corresponding to ENSO phasing are consistent between the three methods (see Figure 1c). For example, consecutive La Niña events in 2010-2012 caused a fall in barystatic sea level (Figure 1c), consistent with Boening et al. (2012). Likewise, significant barystatic sea-level rise during 2015-2016 coincides with strong El Niño conditions (Figure 1c). There are notable disparities between GRACE (∼2.1 mm/yr) and altimetry-based (2.45±0.04 mm/yr) barystatic sea-level trend over the common data period (August 2002 to December 2020). Satellite gravity estimates indicate that barystatic sea-level rise has increased at a slower rate since the launch of GRACE-FO (Figure 1c). Recently, Barnoud et al. (2023) resolved this discrepancy using ocean reanalysis products to compute the thermosteric component of GMSL, suggesting that satellite gravity data have accurately estimated recent trends in barystatic sea level.

5.2 Local sea level changes

According to our computed GRD values, the largest increase in ocean mass caused by continental hydrology occurred around the Gulf of Guinea coast, central-west Africa (Figure 1a,g). The increase in total ocean mass during the GRACE period near Lagos amounts to ∼54 mm, with >40% derived from continental hydrology (Figure 1g). The trend in total manometric sea-level change near Lagos is consistent between GRACE and altimetry-based estimates (∼2.6 mm/yr), indicating insignificant trends in ocean dynamic sea level in this location. Similarly, along the east coast of North America, ice (∼22 mm) and continent-based (∼17 mm) contributions are comparable (compare Figure 1a and b). Interestingly, the GRD contribution from ice-free land areas at New York slowed between 2020 and 2023 due to increased TWS in Asia and Africa (Figure 1h). The average rate of manometric sea-level rise near New York (∼ 2.3 mm/yr) falls within the standard error of trends estimated from satellite gravity and altimetry (Figure 1d).

In contrast, total ocean mass change near Kuwait City in the western Persian Gulf was only ∼15 mm over the 2002-2023 period. Here, the increase due to ice-based contributions (+27 mm) was >40% compensated due to ice-free continental hydrology contributions (-12 mm) (Figure 1e). The significant negative ocean mass signal was mainly driven by Asia, with a ∼2 mm reduction in direct attraction by 2023 due to Caspian Sea water loss. Changes in TWS in Europe had virtually no impact on sea level in the Persian Gulf (pink line in Figure 1i). The ocean mass trend in computed GRD values is small (0.72 mm/yr), accounting for only ∼12% of the trend measured by steric-corrected altimetry near the mouth of the Persian Gulf (Figure 1e). The trend in steric-corrected altimetry and our estimated ocean mascons are in closer agreement at this location, suggesting observable ocean dynamics not captured in computed GRD values are significant (Figure 1e).

Continental hydrology trends were ∼0.5 mm/yr throughout the Pacific island nations, with ice-based contributions typically contributing 70-80% of manometric sea-level rise. During the study period, Kiribati, located in the southwest Pacific Ocean, experienced a total ocean mass increase of 48 mm, of which 10 mm are contributed by non-ice hydrological processes (Figure 1f). Kiribati experienced a high proportion of manometric sea level increase driven by ice mass loss compared to most other Pacific Island nations. Trends in manometric sea level in Kiribati from satellite gravity and altimetry-based estimates are in agreement (∼2.4 mm/yr), suggesting insignificant trends in ocean dynamic sea level (Figure 1f).

Despite significant annual signals in manometric sea level due to TWS changes (Figure 1h-k), magnitudes are small compared to high-frequency dynamic ocean variations recorded in our ocean mascon estimates and steric-corrected altimetry (Figure 1b-e). The amplitude of the annual signal of manometric sea level, as captured by our computed GRD values at New York (6.7 mm), Kuwait City (3.7 mm), Kiribati (11.9 mm), and Lagos (16.1 mm), were dominated (>80%) by the annual signal of TWS changes in ice-free areas. In New York, Kuwait City, and Kiribati, the largest contributions to the annual amplitude originated from TWS changes in South America and Asia, while 40% of the annual amplitude in Lagos originated from the African continent. There is no phase lag between land-based mass changes and ocean mass change in computed GRD values.

5.3 Sea level during consecutive La Niña events

During GRACE/GRACE-FO mission operation, two periods of consecutive La Niña events occurred; 2010-2012 and 2020-2023 (Figure 1c). Both periods resulted in significantly increased rainfall and anomalously high TWS in northern South America and Australia (e.g., Espinoza et al., 2022; Holgate et al., 2022). The rate of GMSL rise slowed significantly from mid-2020 to mid-2022 during the recent triple La Niña, which is characterised by weaker consecutive La Niña events compared to 2010-2012 (Figure 1c). The 2010-2012 and 2020-2023 events removed a total ∼5 mm and ∼3.7 mm of water from the oceans, respectively, and deposited it onto the Australian and northern South American landmasses. During 2010-2012, increased TWS in northern South America and Australia removed 1.09±0.18 mm/yr and 1.4±0.21 mm/yr of GMSL, respectively (Figure 2a,b). In contrast, the recent triple La Niña resulted in a more modest reduction in GMSL due to increased TWS in northern South America and Australia, equivalent to -0.91±0.11 mm/yr and -0.33±0.07 mm/yr GMSL, respectively (Figure 2a,b). These rates were comparable to the long-term contributions of polar ice sheets to GMSL (∼0.39 mm/yr for Antarctica, ∼0.66 mm/yr for Greenland).

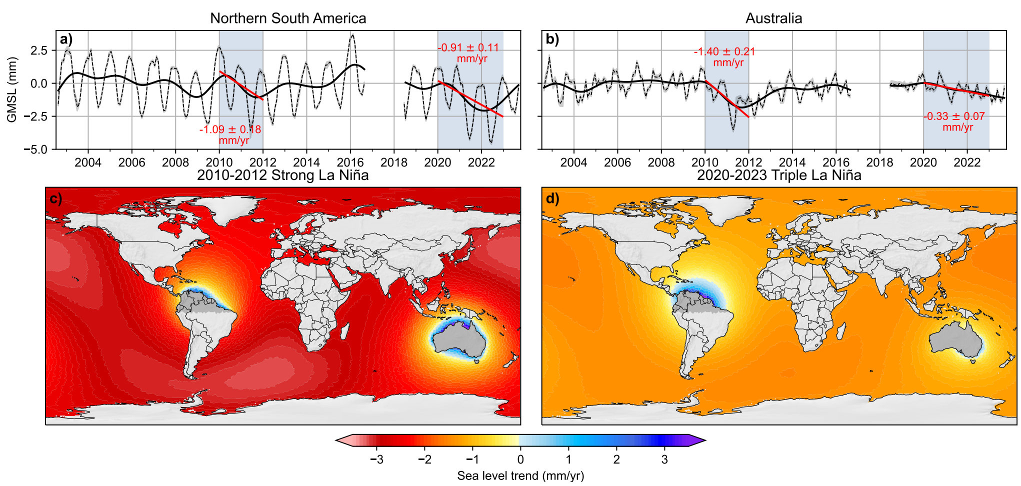

Figure 2. TWS change in equivalent GMSL (dashed line), 24-month low-pass filtered (solid line) and 2010-2012 and 2020-2023 trends (red) for a) northern South America, and b) Australia, respectively. Trend in computed GRD values of ocean mass change derived using sea-level GRD fingerprints to apportion over the oceans the rate of change of TWS for each mascon in Australia and northern South America (dark grey regions) over c) the 2010-2012 and d) 2020-2023 La Niña periods.

Similar spatial patterns of change in manometric sea level resulted during the two periods of consecutive La Niña events that occurred during GRACE and GRACE-FO mission operation (Figure 2c,d). However, the triple La Niña ocean increase was more localised off eastern Australia and the negative ocean mass signals in the far-field oceans were approximately double the magnitude in the earlier event. The increase in ocean mass around the coastline of Australia and northern South America during La Niña periods was due to the stronger direct gravitational attraction of the ocean to the increased water mass on each continent (Figure 2c,d). The southern Atlantic and northern Pacific Oceans lost the most water during the La Niña precipitation events in Australia.

5.4 Anthropogenic impacts on sea level

The growing demand for water resources due to socioeconomic development and population growth resulted in the depletion of TWS in regions reliant on groundwater extraction for crop irrigation (Rodell et al., 2009, 2018). For example, TWS in northern India decreased at 18.7±0.5 Gt/yr (∼0.05 mm/yr GMSL) from 2002 to 2023 (Figure 3a), causing ∼1 mm of barystatic sea-level rise over the study period. Since 2018, the rate of TWS decline in northern India slowed (∼0.02 mm/yr GMSL) despite normal annual precipitation rates (Figure 3a). Northern India groundwater recharge is reliant on low-intensity monsoon season rainfall which has been declining long-term but typically increases during La Niña conditions (Kumar et al., 2006; Asoka et al., 2018), causing a gain in TWS 2010-2012 (Figure 3a). The observed slowing of northern India's contribution to GMSL rise post-2018 is likely the combined effect of increased groundwater recharge during La Niña conditions and decreased extraction rates.

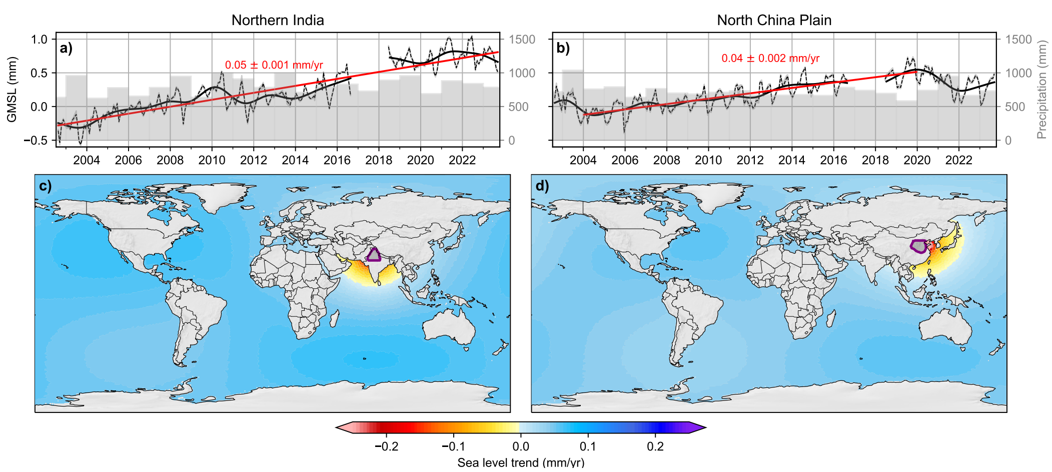

Figure 3. TWS change in equivalent GMSL (dashed line), 24-month low-pass filtered (solid line) and 2002-2023 and 2004-2020 trends (red) for a) northern India, and b) North China Plain, respectively. Corresponding trends in computed GRD values of ocean mass change derived using sea level GRD fingerprints to apportion each of these anthropogenic signals over the oceans (c,d). Mascons used to compute the GRD values are indicated (dark grey, purple line). Grey bars indicate total annual precipitation in mm calculated from ERA5 monthly reanalysis (Hersbach et al., 2019).

Following record precipitation in 2003, TWS in the North China Plain declined at 14.5±0.6 Gt/yr, contributing ∼0.04 mm/yr to GMSL from 2004 to 2020 (Figure 3b). The contribution reverses during the GRACE-FO era, with an increase of 21.1±3.8 Gt/yr in TWS, equivalent to a reduction in GMSL of ∼0.06 mm/yr. This reversal in trend is likely due to the combined effect of significantly increased precipitation in 2021 (Figure 3b) and decreased groundwater abstraction due to agricultural policy reform which resulted in groundwater recharge over the GRACE-FO period (Long et al., 2020; Zhang et al., 2022). Furthermore, the increase in TWS corresponds to reduced industrial water usage during the Covid-19 pandemic (Shu et al., 2023) and increased recharge due to environmental flow releases since 2019 (Liu et al., 2023).

Decreased TWS causes near-field sea-level fall due to reduced gravitational attraction of the oceans to the nearby land mass. Groundwater extraction in northern India increased sea-level between 2002 and 2023 by up to -0.14±0.01 mm/yr along the coastline of southern Pakistan (Figure 3c). Groundwater extraction in the North China Plain

(Rodell et al., 2018) between 2004 and 2020 caused sea-level fall in the East China Sea by up to -0.54±0.02 mm/yr (Figure 3d). Despite a comparable contribution to GMSL rise, this is a factor of ∼4 greater than near-field sea-level fall near southern Pakistan due to groundwater extraction in India because the source is much closer to the coast in China. The peak increases in manometric sea level due to the groundwater extraction in India (2002-2023) and China (2004-2020) occurred in the northwestern Atlantic and Southern Ocean, having the largest impact on sea level in North America and along southern Australian and South African Coastlines (Figure 3d).

6 Conclusion

Natural and anthropogenic hydrological processes in regions that are not ice-covered have contributed to barystatic sea-level rise on multi-decadal time-scales throughout the GRACE/GRACE-FO era. Although they contributed tens of millimetres to manometric sea level in some instances, these impacts are not likely to persist indefinitely. For example, the Asian continent, which contributed to barystatic sea-level rise (2003-2020), has been drawing water from the oceans since 2020. Natural climate variability, such as La Niña events, affect sea level with rates comparable to present day contributions of the polar ice sheets, although these former effects tend to persist for only a few years. Anthropogenic intervention, such as extraction of groundwater resources, increased far-field manometric sea level, but caused decreased local sea level of up to ∼1 mm/yr. These rates of near-field sea-level fall were comparable in magnitude to the longer-term contributions of the polar ice sheets and mountain glaciers, at times masking ∼80% of the sea level increase caused by melting of ice-covered regions. If this extraction of groundwater ceases, then near-field regions (such as the Persian Gulf, eastern Mediterranean, East China Sea, and coastline of southern Pakistan) would see an increase in the rate of local sea-level rise of up to 1 mm/yr, significantly increasing the vulnerability of these regions to sea-level rise. However, if current trends in groundwater abstraction remain, continental hydrology would continue to compound sea-level rise caused by melting of continental ice in the far-field. Currently, over 25% of manometric sea-level rise around Africa, across the central Atlantic Ocean, around Australia and surrounding Pacific Island nations, and in the North Pacific Ocean are due to the declining trend in Asia's TWS between 2002 and 2023.

7 Open Research

The GRACE and GRACE Follow-On Level-1B data used to produce the ANU RL02 solutions are available from `podaac.jpl.nasa.gov/dataset`. The ANU mascon solutions used in this analysis (ANU mascons RL02) and the sea-level fingerprints computed for our mascons are available at [reference added upon acceptance of manuscript]. The barystatic and manometric sea level budget products used in this manuscript were accessed at (Magellium/LEGOS, 2023). Nino3.4 anomalies based on (Rayner et al., 2003) were accessed at (NOAA, 2023) and ERA5 monthly averaged reanalysis products were accessed at (Hersbach et al., 2019).

Acknowledgments
The analysis of the GRACE Follow-On data was funded in part through contracts with Geoscience Australia. R. McGirr was funded by the Australian Research Council Special Research Initiative, Australian Centre for Excellence in Antarctic Science (Project Number SR200100008). We would like to thank Dr Julia Pfeffer and an anonymous reviewer for their insightful comments and constructive feedback, which significantly enhanced the quality of this manuscript.

References

Allgeyer, S., Tregoning, P., McQueen, H., McClusky, S. C., Potter, E.-K., Pfeffer, J., ... Montillet, J.-P. (2022). ANU GRACE data analysis: Orbit modeling, regularization and inter-satellite range acceleration observations. *Journal of Geophysical Research: Solid Earth*, *127*(2), e2021JB022489. doi: 10.1029/2021JB022489

Asoka, A., Wada, Y., Fishman, R., & Mishra, V. (2018). Strong linkage between precipitation intensity and monsoon season groundwater recharge in India. *Geophysical Research Letters*, *45*(11), 5536–5544. doi: 10.1029/2018GL078466

Barnoud, A., Pfeffer, J., Cazenave, A., Fraudeau, R., Rousseau, V., & Ablain, M. (2023). Revisiting the global mean ocean mass budget over 2005–2020. *Ocean Science*, *19*(2), 321–334. doi: 10.5194/os-19-321-2023

Boening, C., Willis, J. K., Landerer, F. W., Nerem, R. S., & Fasullo, J. (2012). The 2011 La Niña: So strong, the oceans fell. *Geophysical Research Letters*, *39*(19). doi: 10.1029/2012GL053055

Chen, J. L., Wilson, C. R., Blankenship, D., & Tapley, B. D. (2009). Accelerated Antarctic ice loss from satellite gravity measurements. *Nature Geoscience*, *2*(12), 859–862. doi: 10.1038/ngeo694

Cheng, L., Trenberth, K. E., Fasullo, J., Boyer, T., Abraham, J., & Zhu, J. (2017). Improved estimates of ocean heat content from 1960 to 2015. *Science Advances*, *3*(3), e1601545. doi: 10.1126/sciadv.1601545

Ciracì, E., Velicogna, I., & Swenson, S. (2020). Continuity of the mass loss of the world's glaciers and ice caps from the GRACE and GRACE Follow-On missions. *Geophysical Research Letters*, *47*(9), e2019GL086926. doi: 10.1029/2019GL086926

Dobslaw, H., Bergmann-Wolf, I., Dill, R., Poropat, L., Thomas, M., Dahle, C., ... Flechtner, F. (2017). A new high-resolution model of non-tidal atmosphere and ocean mass variability for de-aliasing of satellite gravity observations: AOD1B RL06. *Geophysical Journal International*, *211*(1), 263–269. doi: 10.1093/gji/ggx302

Dziewonski, A. M., & Anderson, D. L. (1981). Preliminary reference earth model. *Physics of the earth and planetary interiors*, *25*(4), 297–356. doi: 10.1016/0031-9201(81)90046-7

Espinoza, J.-C., Marengo, J. A., Schongart, J., & Jimenez, J. C. (2022). The new historical flood of 2021 in the Amazon River compared to major floods of the 21st century: atmospheric features in the context of the intensification of floods. *Weather and Climate Extremes*, *35*, 100406. doi: 10.1016/j.wace.2021.100406

Farrell, W., & Clark, J. A. (1976). On postglacial sea level. *Geophysical Journal International*, *46*(3), 647–667. doi: 10.1111/j.1365-246X.1976.tb01252.x

Frappart, F., Papa, F., Güntner, A., Tomasella, J., Pfeffer, J., Ramillien, G., ... others (2019). The spatio-temporal variability of groundwater storage in the Amazon River Basin. *Advances in Water Resources*, *124*, 41–52. doi: 10.1016/j.advwatres.2018.12.005

Good, S. A., Martin, M. J., & Rayner, N. A. (2013). EN4: Quality controlled ocean temperature and salinity profiles and monthly objective analyses with uncertainty estimates. *Journal of Geophysical Research: Oceans*, *118*(12), 6704–6716. doi: 10.1002/2013JC009067

Goux, O., Pfeffer, J., Blazquez, A., Weaver, A. T., & Ablain, M. (2023). A mass conserving filter based on diffusion for gravity recovery and climate experiment (grace) spherical harmonics solutions. *Geophysical Journal International*, *234*(1), 56–72. doi: 10.1093/gji/ggad016

Gregory, J. M., Griffies, S. M., Hughes, C. W., Lowe, J. A., Church, J. A., Fukimori, I., ... others (2019). Concepts and terminology for sea level: Mean, variability and change, both local and global. *Surveys in Geophysics*, *40*, 1251–1289. doi: 10.1007/s10712-019-09525-z

Harvey, N., McCullough, C. M., & Save, H. (2022). Modeling GRACE-FO accelerometer data for the version 04 release. *Advances in Space Research*, *69*(3), 1393–1407. doi: 10.1016/j.asr.2021.10.056

Hersbach, H., Bell, B., Berrisford, P., Biavati, G., Horányi, A., Muñoz Sabater, J., … others (2019). *ERA5 monthly averaged data on single levels from 1979 to present.* Copernicus Climate Change Service (C3S) Climate Data Store (CDS), [Dataset] doi: 10.24381/cds.f17050d7. (Accessed on 19-JAN-2023)

Holgate, C., Evans, J. P., Taschetto, A. S., Gupta, A. S., & Santoso, A. (2022). The impact of interacting climate modes on East Australian precipitation moisture sources. *Journal of Climate*, *35*(10), 3147–3159. doi: 10.1175/JCLI-D-21-0750.1

Jeon, T., Seo, K.-W., Kim, B.-H., Kim, J.-S., Chen, J., & Wilson, C. R. (2021). Sea level fingerprints and regional sea level change. *Earth and Planetary Science Letters*, *567*, 116985. doi: 10.1016/j.epsl.2021.116985

Kim, J.-S., Seo, K.-W., Jeon, T., Chen, J., & Wilson, C. R. (2019). Missing hydrological contribution to sea level rise. *Geophysical Research Letters*, *46*(21), 12049–12055. doi: 10.1029/2019GL085470

Kumar, K. K., Rajagopalan, B., Hoerling, M., Bates, G., & Cane, M. (2006). Unraveling the mystery of Indian monsoon failure during El Niño. *Science*, *314*(5796), 115–119. doi: 10.1126/science.1131152

Lambeck, K., Purcell, A. P., & Zhao, S. (2017). The North American Late Wisconsin ice sheet and mantle viscosity from glacial rebound analyses. *Quaternary Science Reviews*, *158*, 172–210. doi: 10.1016/j.quascirev.2016.11.033

Leblanc, M. J., Tregoning, P., Ramillien, G., Tweed, S. O., & Fakes, A. (2009). Basin-scale, integrated observations of the early 21st century multiyear drought in southeast Australia. *Water Resources Research*, *45*(4). doi: 10.1029/2008WR007333

Legeais, J.-F., Meyssignac, B., Faugère, Y., Guerou, A., Ablain, M., Pujol, M.-I., … Dibarboure, G. (2021). Copernicus sea level space observations: a basis for assessing mitigation and developing adaptation strategies to sea level rise. *Frontiers in Marine Science*, *8*, 704721. doi: 10.3389/fmars.2021.704721

Liu, S., Zhou, Y., Zang, Y., McClain, M. E., & Wang, X.-s. (2023). Effects of downstream environmental flow release on enhancing the groundwater recharge and restoring the groundwater/surface-water connectivity in Yongding River, Beijing, China. *Hydrogeology Journal*, *31*(7), 1795–1811. doi: 10.1007/s10040-023-02675-w

Long, D., Yang, W., Scanlon, B. R., Zhao, J., Liu, D., Burek, P., … Wada, Y. (2020). South-to-North Water Diversion stabilizing Beijing's groundwater levels. *Nature Communications*, *11*(1), 3665. doi: 10.1038/s41467-020-17428-6

Loomis, B. D., Rachlin, K. E., Wiese, D. N., Landerer, F. W., & Luthcke, S. B. (2020). Replacing grace/grace-fo with satellite laser ranging: Impacts on antarctic ice sheet mass change. *Geophysical Research Letters*, *47*(3), e2019GL085488. doi: 10.1029/2019GL085488

Magellium/LEGOS. (2023). *Barystatic and manometric from sea level budget.* Distributed by AVISO+ (https://aviso.altimetry.fr) with support from Copernicus Marine Service [Dataset] doi: 10.24400/527896/a01-2023.012. (Accessed on 07-MAR-2023)

McGirr, R., Tregoning, P., Allgeyer, S., McQueen, H., & Purcell, A. P. (2022). Mitigation of thermal noise in GRACE accelerometer observations. *Advances in Space Research*, *69*(1), 386-401. doi: 10.1016/j.asr.2021.10.055

Mitrovica, J. X., Gomez, N., Morrow, E., Hay, C., Latychev, K., & Tamisiea, M. E. (2011). On the robustness of predictions of sea level fingerprints. *Geophysical Journal International*, *187*(2), 729–742. doi: 10.1111/j.1365-246X.2011.05090

.x

Mitrovica, J. X., Tamisiea, M. E., Davis, J. L., & Milne, G. A. (2001). Recent mass balance of polar ice sheets inferred from patterns of global sea-level change. *Nature*, *409*(6823), 1026–1029. doi: 10.1038/35059054

Muller, P. M., & Sjogren, W. L. (1968). Mascons: Lunar mass concentrations. *Science*, *161*(3842), 680–684. doi: 10.1126/science.161.3842.680

NOAA. (2023). *PSL Download Climate Timeseries, Niño3.4 SST Index.* [Dataset] `https://psl.noaa.gov/gcos_wgsp/Timeseries/Data/nino34.long.anom.data`. (Accessed on 08-AUG-2023)

Peltier, R. W., Argus, D. F., & Drummond, R. (2018). Comment on "an assessment of the ice-6g_c (vm5a) glacial isostatic adjustment model" by purcell et al. *Journal of Geophysical Research: Solid Earth*, *123*(2), 2019–2028. doi: 10.1002/2016JB013844

Rayner, N. A. A., Parker, D. E., Horton, E. B., Folland, C. K., Alexander, L. V., Rowell, D., ... Kaplan, A. (2003). Global analyses of sea surface temperature, sea ice, and night marine air temperature since the late nineteenth century. *Journal of Geophysical Research: Atmospheres*, *108*(D14). doi: 10.1029/2002JD002670

Rodell, M., Famiglietti, J. S., Wiese, D. N., Reager, J., Beaudoing, H. K., Landerer, F. W., & Lo, M.-H. (2018). Emerging trends in global freshwater availability. *Nature*, *557*(7707), 651–659. doi: 10.1038/s41586-018-0123-1

Rodell, M., Velicogna, I., & Famiglietti, J. S. (2009). Satellite-based estimates of groundwater depletion in India. *Nature*, *460*(7258), 999–1002. doi: 10.1038/nature08238

Rowlands, D. D., Luthcke, S. B., Klosko, S. M., Lemoine, F. G. R., Chinn, D. S., McCarthy, J. J., ... Anderson, O. B. (2005). Resolving mass flux at high spatial and temporal resolution using GRACE intersatellite measurements. *Geophysical Research Letters*, *32*(4). doi: 10.1029/2004GL021908

Shu, F., Liu, H., Fu, G., Sun, S., Li, Y., Ding, W., ... others (2023). Unraveling the Impact of COVID-19 Pandemic Dynamics on Commercial Water-Use Variation. *Journal of Water Resources Planning and Management*, *149*(8), 04023036. doi: 10.1061/JWRMD5.WRENG-5940

Sun, J., Wang, L., Peng, Z., Fu, Z., & Chen, C. (2022). The sea level fingerprints of global terrestrial water storage changes detected by GRACE and GRACE-FO data. *Pure and Applied Geophysics*, *179*(9), 3493–3509. doi: 10.1007/s00024-022-03123-8

Sun, Y., Riva, R., & Ditmar, P. (2016). Optimizing estimates of annual variations and trends in geocenter motion and J_2 from a combination of GRACE data and geophysical models. *Journal of Geophysical Research: Solid Earth*, *121*(11), 8352–8370. doi: 10.1002/2016JB013073

Tamisiea, M., Hill, E., Ponte, R., Davis, J., Velicogna, I., & Vinogradova, N. (2010). Impact of self-attraction and loading on the annual cycle in sea level. *Journal of Geophysical Research: Oceans*, *115*(C7). doi: 10.1029/2009JC005687

Tapley, B. D., Bettadpur, S., Watkins, M., & Reigber, C. (2004). The gravity recovery and climate experiment: Mission overview and early results. *Geophysical research letters*, *31*(9). doi: 10.1029/2004GL019920

Tapley, B. D., Watkins, M. M., Flechtner, F., Reigber, C., Bettadpur, S., Rodell, M., ... others (2019). Contributions of GRACE to understanding climate change. *Nature climate change*, *9*(5), 358–369. doi: 10.1038/s41558-019-0456-2

Tregoning, P., McGirr, R., Pfeffer, J., Purcell, A. P., McQueen, H., Allgeyer, S., & McClusky, S. C. (2022). ANU GRACE data analysis: Characteristics and benefits of using irregularly shaped mascons. *Journal of Geophysical Research: Solid Earth*, *127*(2), e2021JB022412. doi: 10.1029/2021JB022412

Velicogna, I., & Wahr, J. (2006). Measurements of time-variable gravity show mass loss in Antarctica. *science*, *311*(5768), 1754–1756. doi: 10.1126/

science.1123785
Velicogna, I., & Wahr, J. (2013). Time-variable gravity observations of ice sheet mass balance: Precision and limitations of the GRACE satellite data. *Geophysical Research Letters*, *40*(12), 3055–3063. doi: 10.1002/grl.50527
Watkins, M. M., Wiese, D. N., Yuan, D.-N., Boening, C., & Landerer, F. W. (2015). Improved methods for observing Earth's time variable mass distribution with GRACE using spherical cap mascons. *Journal of Geophysical Research: Solid Earth*, *120*(4), 2648–2671. doi: 10.1002/2014JB011547
Wiese, D. N., Landerer, F. W., & Watkins, M. M. (2016). Quantifying and reducing leakage errors in the JPL RL05M GRACE mascon solution. *Water Resources Research*, *52*(9), 7490–7502. doi: 10.1002/2016WR019344
Wouters, B., Gardner, A. S., & Moholdt, G. (2019). Global glacier mass loss during the GRACE satellite mission (2002-2016). *Frontiers in Earth Science*, *7*, 96. doi: 10.3389/feart.2019.00096
Zhang, Y., Zhou, W., Wang, X., Chen, S., Chen, J., & Li, S. (2022). Indian Ocean Dipole and ENSO's mechanistic importance in modulating the ensuing-summer precipitation over Eastern China. *npj Climate and Atmospheric Science*, *5*(1), 48. doi: 10.3389/feart.2019.00096

Figure 1.

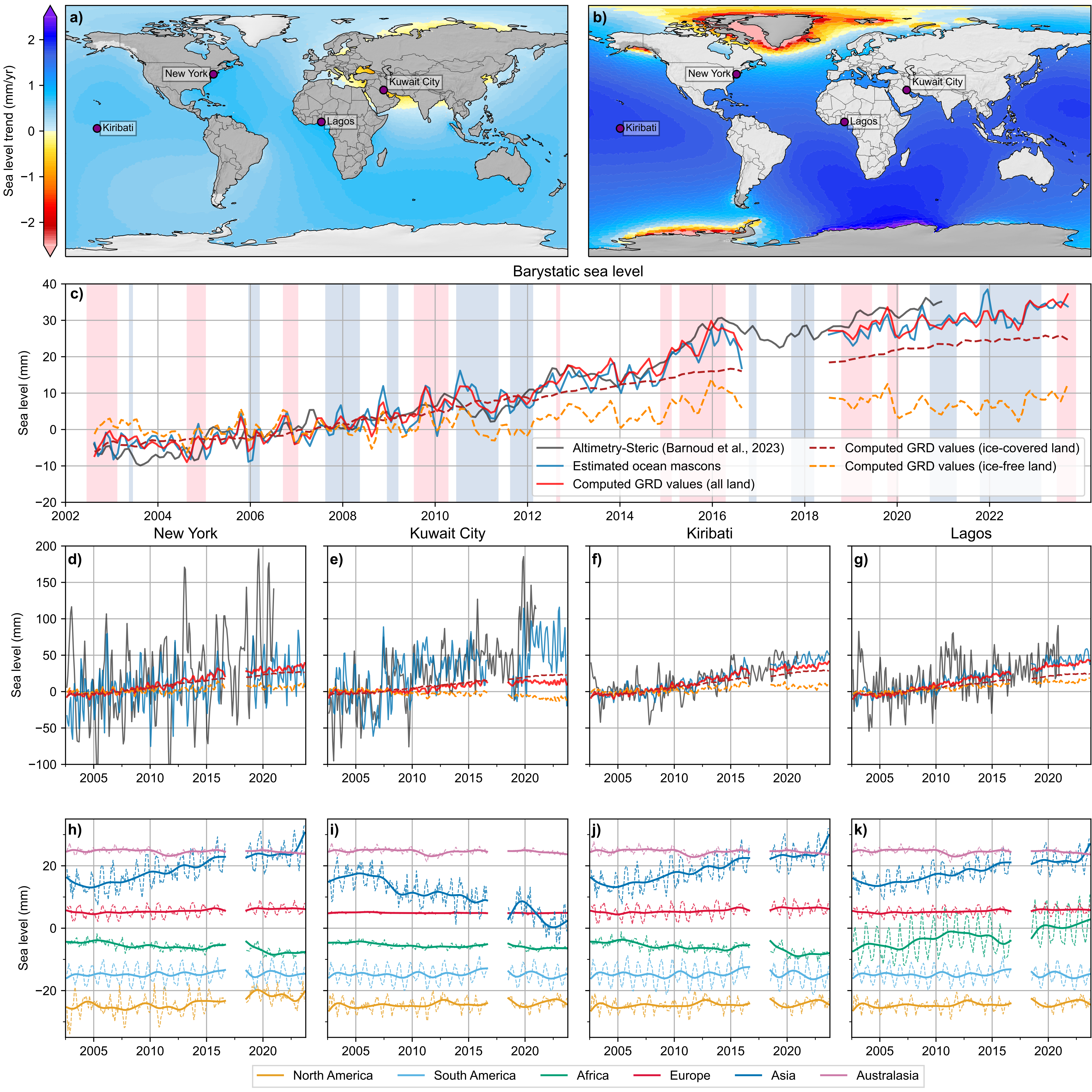

a)
b)
Sea level trend (mm/yr)
New York
Kuwait City
Kiribati
Lagos
Barystatic sea level
c)
Sea level (mm)
Altimetry-Steric (Barnoud et al., 2023)
Estimated ocean mascons
Computed GRD values (all land)
Computed GRD values (ice-covered land)
Computed GRD values (ice-free land)
New York
Kuwait City
Kiribati
Lagos
d)
e)
f)
g)
h)
i)
j)
k)
North America
South America
Africa
Europe
Asia
Australasia

Figure 3.

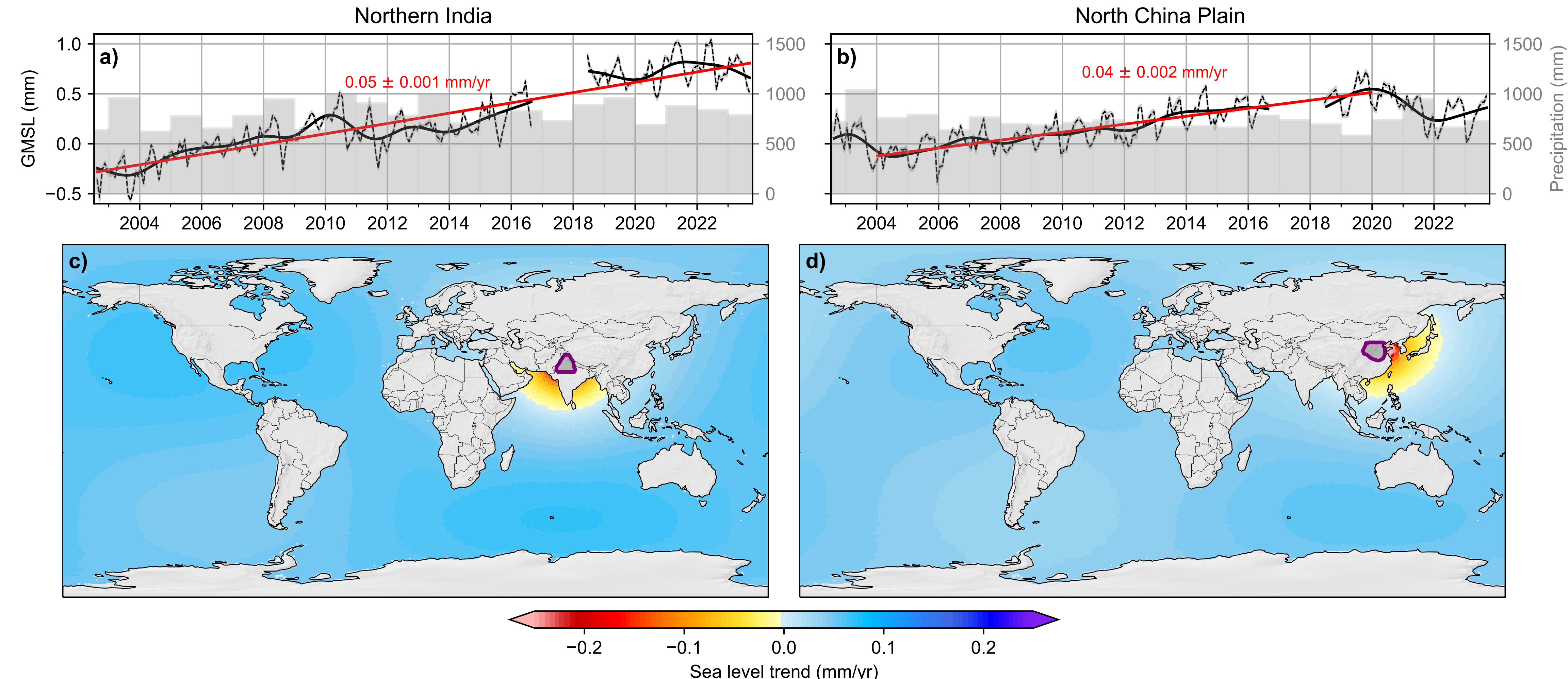
Northern India
North China Plain
a)
b)
c)
d)
0.05 ± 0.001 mm/yr
0.04 ± 0.002 mm/yr
GMSL (mm)
Precipitation (mm)
1.0
0.5
0.0
−0.5
1500
1000
500
0
2004
2006
2008
2010
2012
2014
2016
2018
2020
2022
−0.2
−0.1
0.0
0.1
0.2
Sea level trend (mm/yr)

Figure 2.

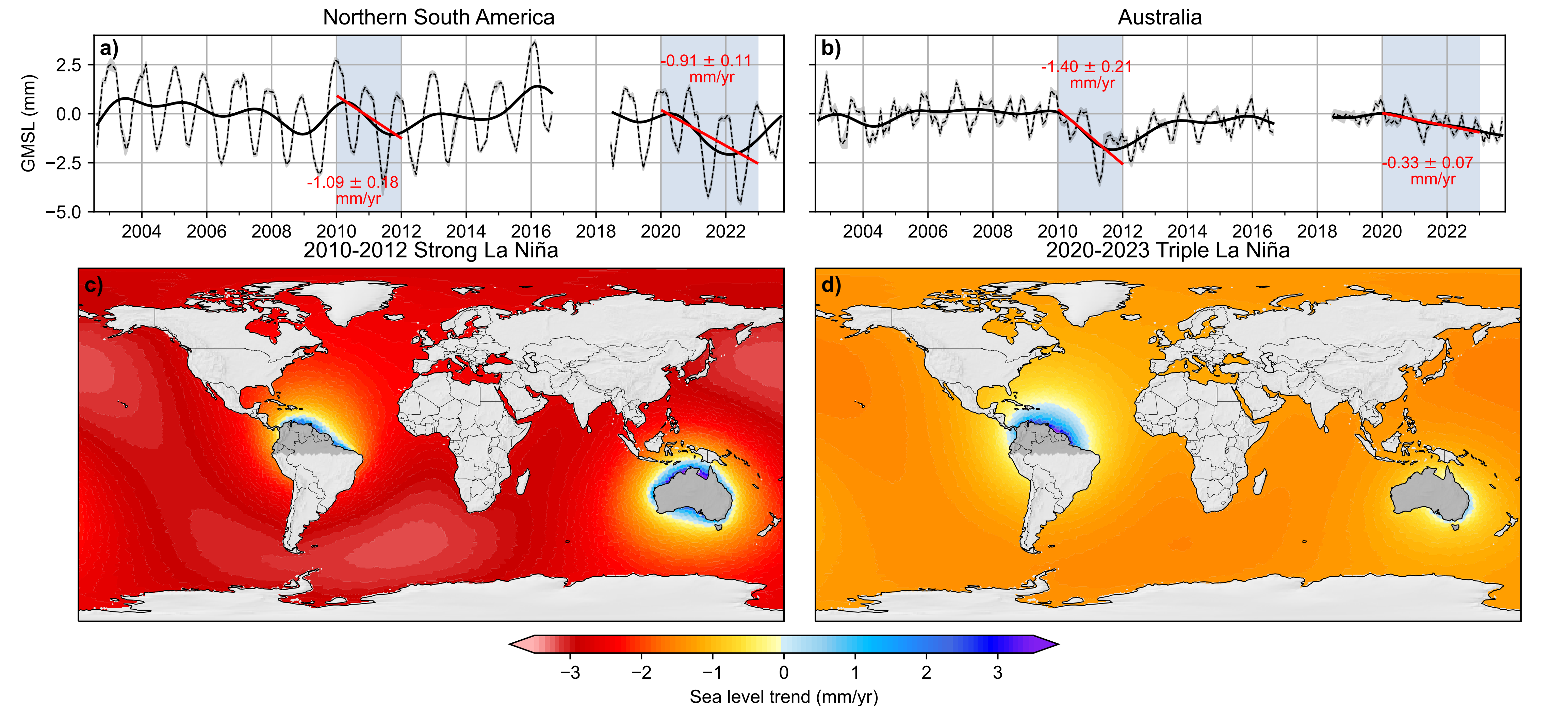
Northern South America
Australia
a)
b)
GMSL (mm)
2.5
0.0
−2.5
−5.0
-0.91 ± 0.11
mm/yr
-1.09 ± 0.18
mm/yr
-1.40 ± 0.21
mm/yr
-0.33 ± 0.07
mm/yr
2004
2006
2008
2010
2012
2014
2016
2018
2020
2022
2010-2012 Strong La Niña
2020-2023 Triple La Niña
c)
d)
−3
−2
−1
0
1
2
3
Sea level trend (mm/yr)